Journal of the Energy Institute 93 (2020) 1229–1241

Contents lists available at ScienceDirect

Journal of the Energy Institute

journal homepage: www.journals.elsevier.com/journal-of-the-energy-institute

Chemical looping combustion of lignite with the $CaSO_4$–CoO mixed oxygen carrier

Baowen Wang [a, c, *], Heyu Li [a], Wei Wang [a], Cong Luo [c], Daofeng Mei [b]

[a] Research Institute for Coal Clean and Efficient Utilization, College of Electric Power, North China University of Water Resources and Electric Power, Zhengzhou, 450045, China
[b] College of Engineering, Huazhong Agricultural University, Wuhan, 430070, China
[c] State Key Laboratory of Coal Combustion, Huazhong University of Science and Technology, Wuhan, 430074, China

ARTICLE INFO

Article history:
Received 3 July 2019
Received in revised form
10 November 2019
Accepted 11 November 2019
Available online 19 January 2020

Keywords:
Coal
Chemical looping combustion
$CaSO_4$–CoO mixed OC
Decarbonization
Desulfurization

ABSTRACT

Chemical looping combustion (CLC) has well developed as a novel combustion technology for simultaneous completion of the coal combustion and CO_2 capture with a low energy penalty. Among all the oxygen carriers available, $CaSO_4$ has gained great attention as a promising oxygen carrier (OC) in CLC due to its high oxygen capacity and low price. But further application of $CaSO_4$ OC also suffers the problems of low reactivity and even deactivation due to the sulfur loss via the side reactions of $CaSO_4$, which should be well addressed. In this research, the $CaSO_4$–CoO mixed OC was prepared firstly, and experiments based on thermogravimetric analyzer coupled with Fourier transform infrared spectroscopy (TG-FTIR) were conducted to evaluate the reaction characteristics and evolution of the gaseous products during the reaction of the prepared $CaSO_4$–CoO mixed OC with lignite (abbreviated as YN). Both the higher reaction rate of the prepared mixed OC with YN coal and the elevated CO_2 concentration fully reflected the enhanced reactivity of the prepared mixed OC for YN coal conversion. Furthermore, the micromorphology of the solid reaction products was analyzed by the field emission scanning electron microscopy spectrometry (FESEM). Good sintering resistance of the prepared $CaSO_4$–CoO mixed OC during its reaction with YN was verified, which was ascribed to the temporary inert support role played by the $CaSO_4$ substrate. In order to further study the desulfurization ability of CoO in the mixed OC, X-ray diffraction (XRD), X-ray photoelectron spectroscopy (XPS) and thermodynamic simulation were used for in-depth analysis. The gaseous sulfur species released by the $CaSO_4$ side reactions were mainly fixed as solid CoS, Co_9S_8 and CaS, with the total content higher than 99.8%. And the sulfided OC could be completely regenerated to its original state at the oxidation stage according to the X-ray diffraction (XRD) result. Overall, the prepared $CaSO_4$–CoO mixed OC not only has the enhanced reactivity and good sintering resistance, but also owns the potential to control sulfur released from the $CaSO_4$ side reactions, which has broad application prospect to simultaneously achieve decarbonization and desulfurization in the CLC process.

1. Introduction

With the global warming problem becoming more and more serious, effective measures must be taken to control and reduce the emitted greenhouse gases, especially for CO_2 from coal combustion. Among all the carbon capture technologies, including post combustion, precombustion and oxyfuel combustion, chemical looping combustion (CLC) technology is achieving a great interest due to its inherent carbon capture with a minimal energy penalty [1]. In a CLC system, reactive oxygen carrier (OC) is used to replace the air for coal oxidation and circulated between the fuel reactor (FR) and the air reactor (AR). If efficient conversion of fuel is reached, after simple condensation, high-purity of the CO_2 stream could be easily obtained at the outlet of the FR. Considering the coal-based energy structure in China, it is of great significance for China to actively develop coal-fuelled CLC so as to achieve efficient and clean utilization of coal resources [2].

* Corresponding author. Research Institute for Coal Clean and Efficient Utilization, College of Electric Power, North China University of Water Resources and Electric Power, Zhengzhou, 450045, China.
E-mail address: david-wn@163.com (B. Wang).

https://doi.org/10.1016/j.joei.2019.11.006
1743-9671/

In a real CLC process, OC not only transfers oxygen from the AR to the FR for oxidation of coal, but also acts as heat carrier to maintain the heat balance between the two interconnected reactors. Therefore, the OC should satisfy several requirements before its practical application, including sufficient oxygen transfer capacity, excellent reactivity, high mechanical strength, good resistance to agglomeration and sintering, environmental benignity and low cost [3].

To date, transition metal oxides such as CuO, Fe_2O_3, NiO, CoO and Mn_3O_4 have been extensively studied because of their high reactivity, but utilization of these metal OCs may be limited by relatively high cost and the potential secondary environmental pollution [4,5]. Although some inexpensive natural ores such as hematite, ilmenite and perovskite possess the potential to be used in CLC, the oxygen transfer capacity of these natural ores is really low [6,7].

Compared with those metal OCs above, the $CaSO_4$ OC is becoming attractive for the future commercial application in CLC because of its outstanding oxygen transport capacity, low cost and wide availability [8]. After all, it is the major component of natural gypsum ores and industrial by-products originating from flue gas desulfurization etc [9]. Besides, its reduced state CaS has a high reaction enthalpy with the molecular oxygen present in air to achieve great OC regeneration for the ensuing cyclic utilization [10].

Nevertheless, a drawback to application of $CaSO_4$ as an OC is encountered with the possible emission of gaseous sulfur from $CaSO_4$ reduction and the CaS oxidation by the side reactions Eqs. (1)–(6) below, as illustrated in many previous investigations [11,12]. The sulfur released will not only lead to the atmospheric pollution, but also reduce the purity of the outlet CO_2. What's worse, these side reactions will cause a rapid decline in the $CaSO_4$ reactivity for its cyclic use in CLC.

$$CaSO_4 + H_2 \rightarrow CaO + H_2O + SO_2 \quad (1)$$

$$CaSO_4 + CO \rightarrow CaO + CO_2 + SO_2 \quad (2)$$

$$4CaSO_4 + CH_4 \rightarrow 4CaO + CO_2 + 2H_2O + 4SO_2 \quad (3)$$

$$CaSO_4 + CH_4 \rightarrow CaO + CO_2 + H_2O + H_2S \quad (4)$$

$$3CaSO_4 + CaS \rightarrow 4CaO + 4SO_2 \quad (5)$$

$$CaS + 3/2O_2 \rightarrow CaO + SO_2 \quad (6)$$

To well address the emission of sulfur, two approaches have been proposed. One method is the addition of limestone [13,14], $CaCO_3$ [15] or CaO [16,17] as the sorbent to capture sulfur and decrease its release during the reduction/oxidation process. Another way is to introduce some active transition metal oxides in $CaSO_4$ for desulfurization, such as Fe_2O_3 or CuO or NiO. On the one hand, only lowering reaction temperature without adding the active oxides above has the possibility of inhibiting the side reactions of $CaSO_4$ listed above [18], but the conversion efficiency of coal decreases. On the other hand, active metal oxides as mentioned above own great desulfurization capacity as well as high reactivity for coal conversion. And adding these oxides could suppress the sulfur release and ensures sufficient conversion of coal at the relatively low reaction temperature [19]. Therefore, simultaneous realization of the in-situ desulfurization and decarbonization was possible [12,20,21], which was much meaningful to be applied in the real CLC process. Tian et al. [21] have investigated the reactivity behavior of $CaSO_4$ OC with coal chars when impregnating with Ni or Fe ions. The reaction activity was remarkably improved after impregnation, and high impregnation fraction of nickel or iron ions is beneficial to the reactivity of $CaSO_4$ OC. Wang et al. [22] have studied the reaction characteristics of $CaSO_4$–CuO mixed OC, which showed that addition of CuO could greatly improve the reactivity of $CaSO_4$, and also effectively inhibit the release of sulfur through the side reactions. However, other transition metal oxides, such as CoO, may also own the good potential to inhibit gaseous sulfur emissions [23], but the current research on the $CaSO_4$–CoO is still limited.

Therefore, in this research, CoO modified $CaSO_4$ OC was firstly prepared and its reaction characteristics with lignite (YN) were systematically investigated by thermogravimetric analysis (TGA) and further quantitatively evaluated. The gaseous composition of flue gas emitted from the TGA was detected online using Fourier transform infrared spectrometer (FTIR), while the solid products formed were analyzed using field emission scanning electron microscopy/energy-dispersive X-ray spectroscopy (FESEM-EDX), X-ray diffraction (XRD) and X-ray photoelectron spectroscopy (XPS). Finally, as a good supplement to the experiments above, thermodynamic simulation of the as-prepared $CaSO_4$–CoO mixed OC reaction with YN was conducted. And the effects of different factors on the migration and transformation of sulfur components, including temperature, CoO/$CaSO_4$ mass ratio and OC addition, were focused.

2. Experimental section

2.1. Materials and characterization

The particles of $CaSO_4$–CoO mixed OC at the mass ratio of 6:4 were firstly prepared by the template method combined with the sol-gel combustion synthesis (SGCS) as developed by our group before [24]. This preparation method not only had great advantages of the template method in structural, morphological and dimensional controllability for nanomaterials synthesis [25,26], but also obtained the rapid, efficient and convenient characteristics of SGCS method in the preparation of OCs with high reactivity and sintering resistance [24,27]. Based on these methods, we have successfully synthesized a variety of high performance OCs, including $CaSO_4$–CuO [22] and $CaSO_4$–Mn_3O_4 [28], which proved the excellent reactivity of the prepared OC in coal conversion and good desulfurization of the gaseous sulfur emitted from the $CaSO_4$ side reactions. The major procedures were listed as followed. A Chinese natural anhydrite ore ($CaSO_4$, over 95 wt%) was crushed, sieved to around 100 μm and adopted as the substrate template. Based on the propellant chemistry theory [29] with consideration of the low contents of the impurities involved, both $Co(NO_3)_2 \cdot 6H_2O$ of analytical reagent (AR) grade (≥98.5 wt%), urea of AR grade (>98 wt%) and the as-prepared $CaSO_4$ particles were dissolved together in deionized (DI) water at the fixed molar ratio as 1, 2.5 and 0.83, respectively. After magnetic stirring in a stirrer of high power (88-1, Guohua Co., China), drying in a DZG-6020D vacuum drying chamber (Senxin company, China), igniting and sintering in a muffle furnace (KF 1200, Nanjing BYT Co., China), the calcined $CaSO_4$–CoO mixed OC was ground using a lab ball grinder XGB04 (Nanjing BYT Co., China) and sieved via a vibrating sieving device (SIEVEA 502, Dandong HMK Instrument Co., China) to 63–106 μm for use.

As sulfur is one of the main elements in coal, its occurrence and evolution may interfere the subsequent investigation of the side reactions of $CaSO_4$ during the reaction of the $CaSO_4$–CoO mixed OC with YN. In order to minimize the detrimental influences of various sulfur compounds involved in coal, a typical lignite collected from Indonesia (abbreviated as YN) was chosen and grinded to 63–106 μm in this research, in which the ash and sulfur contents were quite low, as provided in Table 1.

To achieve the full conversion of YN coal, it is important to

Table 1
Properties of Indonesia lignite (YN) sample.

Proximate analysis (wt %)				Ultimate analysis (wt %, ad[b])						
M_{ad}[a]	V_{ad}[a]	A_{ad}[a]	FC_{ad}[a]	C	H	N	S	O[c]	LHV[d](MJ/kg)	
6.06	49.69	4.63	39.62	71.13	4.64	0.94	0.13	12.47	18.36	
Ash analysis (wt %)										
SiO_2	Al_2O_3	Fe_2O_3	SO_3	CaO	TiO_2	MnO	K_2O	MgO	Na_2O	Total
48.80	19.59	12.62	1.25	6.04	1.06	0.32	1.70	4.55	0.40	96.01

[a] M: moisture content; V: volatile matters; A:ash content; FC: fixed carbon; ad: air-dried basis.
[b] Dry basis.
[c] The O content was determined by difference.
[d] Lower heating value.

determine the supply of the $CaSO_4$–CoO mixed OC firstly [30,31]. When only the major elements (C, H, S, O and N) are considered, the relative chemical formula of 1 kg YN lignite can be determined as $C_{53.2}H_{34.9}S_{0.04}O_{7.2}N_{0.6}$ according to the proximate and ultimate analysis shown in Table 1 above. Assuming that 1 kg YN coal was just stoichiometrically oxidized by the $CaSO_4$–CoO while the $CaSO_4$–CoO was mainly reduced to CaS and elemental Co, respectively, the $CaSO_4$–CoO oxygen excess number could be defined as the unity. Therefore, the mass ratio of $CaSO_4$–CoO to YN coal was determined as 5.08. While for the two reference oxides, $CaSO_4$ and CoO, their mass ratios to YN coal could be calculated as 3.96 and 8.75, respectively.

2.2. Experimental methods

Reaction characteristics of the $CaSO_4$–CoO mixed OC with YN lignite were investigated using a thermogravimetric analyzer (TG 209 F3, Netzsch Corp., Germany). About 15 mg of the mixture of $CaSO_4$–CoO and YN at the fixed mass ratio mentioned above was heated from the ambient temperature to 900 °C at 25 °C/min, and then remained at this final temperature for 15 min to ensure the sufficient conversion of coal. To avoid the potential impact of the introduced CO_2 or H_2O on the subsequent FTIR analysis, N_2 atmosphere was used as the reaction atmosphere to simplify the experimental process, as many researchers have adopted [32–34]. The flow rate of N_2 was set at 80 mL/min to ensure the reproducibility of the experimental results and also to overcome the adverse effects of heat and mass transfer. In addition, the YN coal pyrolysis under N_2 atmosphere and its reaction with the single CoO and $CaSO_4$ were performed at the same experimental conditions for reference.

The Fourier transform infrared spectrometer (FTIR) as EQUINOX 55 (Bruker Corp., Germany) was employed to on-line detect the gases evolved from YN coal reaction with the $CaSO_4$–CoO mixed OC in the TGA. The morphology and elemental composition of the solid products from the reaction of YN with $CaSO_4$–CoO were studied by the field emission scanning electron microscopy (FESEM) spectrometer Siron 200 (FEI Company, Netherlands) coupled with an energy-dispersive X-ray spectrometer (EDX) as Genesis (EDAX Corp., USA). And the crystalline phases as formed were identified by X-ray diffraction (XRD) using X'Pert PRO (PANalytical Corp.,Netherlands) subsequently. Finally, the chemical states and surface compositions of the solid products were analyzed by an X-ray photoelectron spectroscopy (XPS) as VG MultiLab 2000 (Thermo Electron Corp., USA) with a monochromatic Mg Kα source and a charge neutralizer. All of the obtained binding energies were referenced to the C 1s peak at 284.6 eV and further decovoluted using the commercial software affiliated to the XPS spectrometer.

2.3. Thermodynamic simulation of YN reaction with the $CaSO_4$–CoO mixed OC

As to thermodynamic simulation, it was known to have the inherent deficiency and does not consider the kinetic constraints of the reaction system, including turbulent mixing and temperature gradients. But it is to enable a better understanding of the complex interaction, oxygen transformation and sulfur migration for YN reaction with the $CaSO_4$–CoO mixed OC. And thus, it is a good supplement to the experiments above. In this research, based on the minimization theorem of Gibbs free energy, a commercial software HSC Chemistry was used to simulate the reaction characteristics of the $CaSO_4$–CoO mixed OC with YN. And the calculation procedures were listed below.

According to the properties of YN coal in Table 1, including its proximate and ultimate analysis as well as ash analysis, a more complex reaction system was established for YN coal reaction with the $CaSO_4$–CoO mixed OC. The main organic matrix (such as C, H, N, S and O) as well as the potential minerals included was established for YN coal. While both the reduced mixed OC and the possible intermediates with the YN minerals were considered so as to make the equilibrium simulation more realistic. Furthermore, in order to realize in-situ fixation of the gaseous sulfur released from the $CaSO_4$ side reactions, effects of different factors (including the reaction temperature, CoO/$CaSO_4$ mixed ratio and the OC excess number) on the migration and transformation of sulfur species for YN coal reaction with the mixed OC was thermodynamically studied as well.

3. Result and discussion

3.1. TGA-FTIR investigation of the reaction of $CaSO_4$–CoO with YN coal

Reaction of YN coal with the $CaSO_4$–CoO mixed OC under N_2 atmosphere was performed using the thermogravimetric analyzer (TGA), and the gaseous products evolved from the coupled TGA were introduced to the FTIR spectrometer for online analysis. Meanwhile, as a reference, the conventional combustion of YN coal in air and its reaction with the two reference oxides, CoO and $CaSO_4$, were performed as well. The experimental results of the weight loss (TG) and the differential weight loss rates (DTG) were presented in Fig. 1, while the gaseous products were detected by the FTIR spectrometer and their evolution as a function of the reaction time was shown in Fig. 2.

Firstly, the combustion of YN lignite in air was conducted. The TG and DTG curves were shown in Fig. 1(a)–(b), respectively. It could be observed that after dehydration, the TG curve declined rapidly and maintained at 2.6% in the end, slightly lower than the

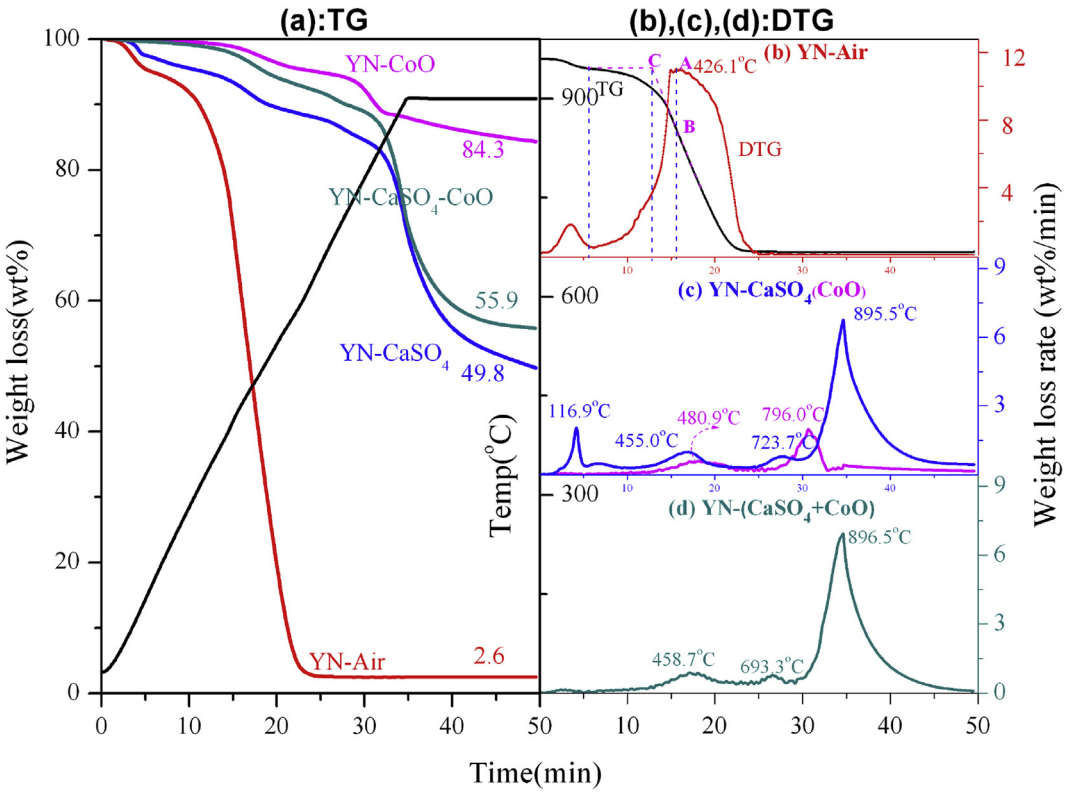

Fig. 1. Reaction characteristics of YN with the $CaSO_4$–CoO mixed OC: (a) weight loss; (b) weight loss rate of YN combustion in air; (c) weight loss rate of YN reaction with the reference $CaSO_4$ or CoO; (d) weight loss rate of YN reaction with the mixed $CaSO_4$–CoO.

proximate analysis result (4.63%), which was mainly due to the experimental condition difference, including the reaction temperature and the different reaction durations experienced. In addition to the dehydration peak below 200 °C, there was a single broad peak in the DTG curve for YN combustion, which corresponded to the intense combustion of the carbon matrix in YN, with the maximum weight loss rate reaching as high as 11.01%/min. According to the Beer-Lambert's Law, gas concentration could be judged from its absorbance intensity due to their linear relation as specified [35]. Therefore, the concentration of gaseous products could be directly inferred by the FTIR absorbance intensity. From Fig. 2(a), CO_2 and H_2O were the main gaseous products during YN combustion in air. As accompanied, a little CO and light hydrocarbon gas CH_4 occurred at the same reaction range. Meanwhile, thanks to the low sulfur content of YN coal adopted in this research, SO_2 was hardly detected during combustion, which was advantageous to avoid the interference of sulfur components involved in coal to the subsequent experiments as expected.

When adding the mixed $CaSO_4$–CoO and its reference oxides CoO and $CaSO_4$, the reaction of YN coal changed greatly, as shown in Fig. 1(a), (c) and (d). From the related TG and DTG curves for the reaction of YN coal with the reference oxide CoO, the residual TG value left for YN coal reaction with CoO was 84.3 wt%, and two reaction stages were presented at the peak temperatures 480.9 and 796.0 °C, respectively. Correspondingly, the maximal weight loss rate reached 0.5990 and 1.9855 wt%/min, respectively. Meanwhile, only two CO_2 and H_2O signal peaks could be observed in the FTIR spectra as presented in Fig. 2(b), which corresponded to the two reaction stages mentioned above. Obviously, the reaction temperature had a great influence on the conversion efficiency of YN coal and more residual char reacted with CoO at the higher temperature [36].

While for the reaction of YN with the reference $CaSO_4$ as shown in Fig. 1(b), apart from the fast dehydration of the adsorbed water in $CaSO_4$ at the peak 116.9 °C [37], three reaction stages could be observed with the peak temperatures residing at 455.0, 723.7 and 895.6 °C, respectively. According to the emitted reducible gases as CH_4 and CO shown in Fig. 2(c), the first stage for YN reaction with the reference $CaSO_4$ at the peak temperature 455.0 °C was ascribed to pyrolysis of YN alone, far different from YN reaction with the reference CoO studied above. This result fully demonstrated the higher reactivity of CoO than that of $CaSO_4$. And addition of CoO could be conducive to enhancing the reactivity of $CaSO_4$. As followed, reductive decomposition of $CaSO_4$ with YN started at the sequential peak temperatures around 723.7 and 895.6 °C, which were higher than the reported temperature values by Yani and Zhang for an Australian lignite with $CaSO_4$ [38], but lower than the value reported by Zheng et al. [39] for reductive decomposition of the gypsum obtained from the desulfurization process by anthracite. And such findings mainly resulted from the differences in the coal and $CaSO_4$ samples, their mixing mode and the reaction conditions. From the FTIR spectra of Fig. 2(c), in addition to the obvious peaks of CO_2 and H_2O, the SO_2 signal derived from the side reactions of $CaSO_4$ was also detected by the FTIR spectrometer, mainly occurring at the latter reaction stage. And the relative concentration of SO_2 increased with the reaction temperature, which was consistent with the findings of other researchers [10,13]. The sulfur released was harmful to the environment, the purity of the outlet CO_2 and the reactivity of $CaSO_4$ as clarified above. And effective measures should be taken to well address this problem.

As to the reaction of YN coal with the prepared $CaSO_4$–CoO mixed OC, from Fig. 1(a) and (d), it could be observed that three main reaction stages occurred in the real profile of the weight loss rate as formed in Fig. 1(d). And the residual amount after reaction

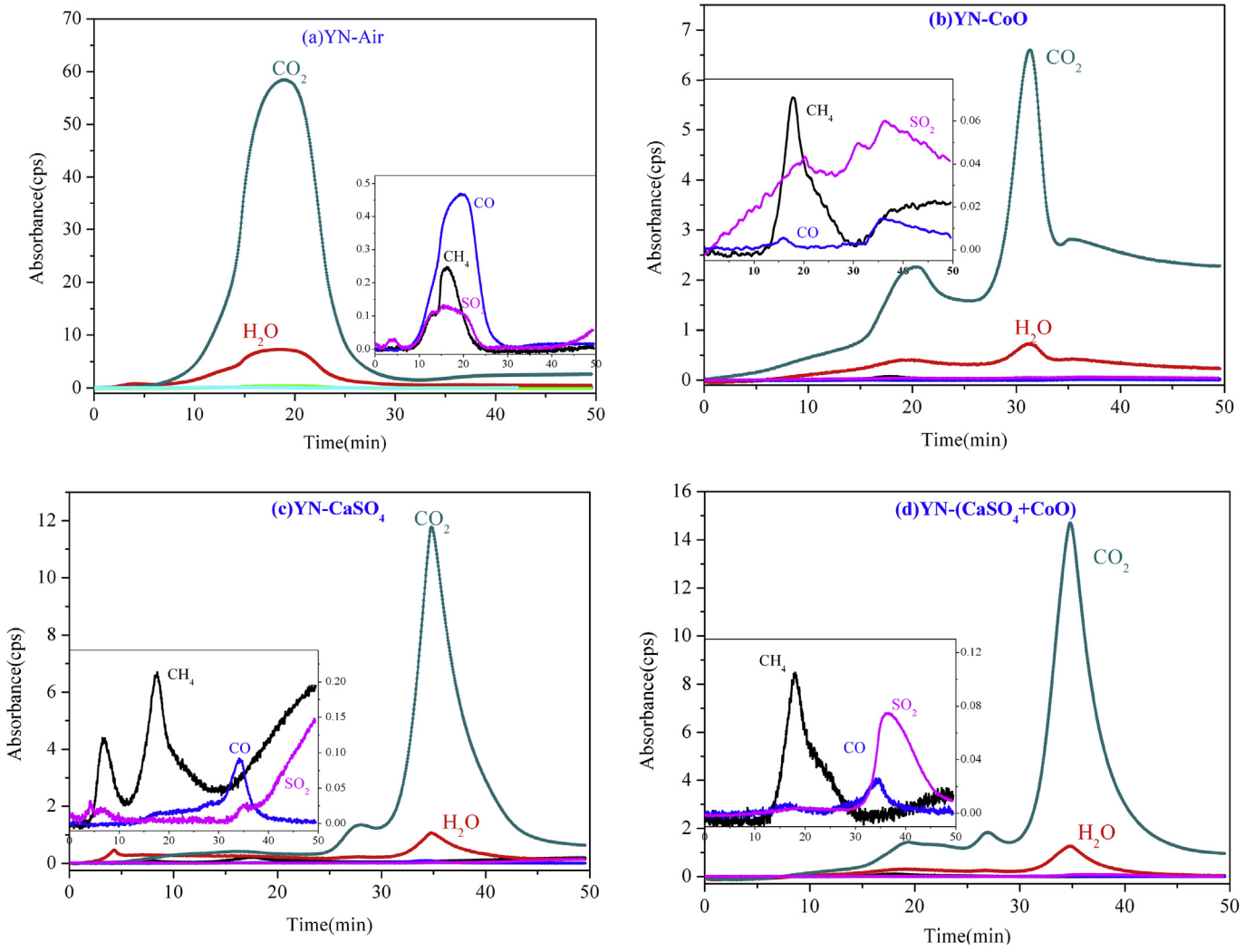

Fig. 2. FTIR spectra for the gaseous products evolved: (a) YN combustion in air; (b) YN reaction with CoO; (c) YN reaction with $CaSO_4$; (d) YN reaction with the mixed $CaSO_4$–CoO.

reached 55.9%. For the first two reaction stages, it mainly originated from the reaction between the pyrolysis products of YN coal with CoO and $CaSO_4$, respectively. And the corresponding peak temperatures (458.7 and 693.3 °C) were lower than those of YN reaction with the reference CoO (480.9 °C) and $CaSO_4$ (723.7 °C), which meant that the individual components in the mixed OC owned higher reactivity due to the combined preparation method applied in this research as well as the possible reaction synergism between the two single components. Furthermore, at the third reaction stage for YN with the $CaSO_4$–CoO mixed OC, the reaction peak temperature was moved to 896.5 °C, which is basically the same as that of YN reaction with the reference $CaSO_4$. But the maximal weight loss rate reached to 6.95 wt%/min, much higher than that of YN with the reference $CaSO_4$ (6.78 wt%/min). In the meantime, as can be seen from the FTIR spectra of Fig. 2(d), during YN reaction with the $CaSO_4$–CoO mixed OC, the main gaseous products were identified to be CO_2 and H_2O. And the triple-peak CO_2 profile was formed and ascribed to the sequential reaction of YN with CoO and $CaSO_4$ at the different stages as discussed in Fig. 1 above. And thus, adding the high active CoO to the $CaSO_4$, the CO_2 peak signal at the third stage increased significantly, which kept the consistency with the TG experimental results shown in Fig. 1(d). This may be due to the innovative preparation method in this study, which enabled the high active CoO grains closely distributed around the $CaSO_4$ substrate. And thus, the reduced metal Co could recover the lattice oxygen from the unreacted $CaSO_4$ at the ionic state and was further oxidized to Co_3O_4, similar to our previous research on the YN reaction with $CaSO_4$–CuO [22] and with $CaSO_4$–Mn_3O_4 mixed OC [28], respectively. But the maximal weight loss rate at this final reaction stage for YN reaction with $CaSO_4$–CoO was nearly equal to that of YN with $CaSO_4$–Mn_3O_4, and was much higher than that of YN with $CaSO_4$–CuO, which indicated the good application potential of the prepared $CaSO_4$–CoO mixed OC in the realistic CLC system. And the newly formed Co_3O_4, with the oxygen uncoupling characteristic, could decompose O_2 for the direct combustion of YN char residue, which was of great interest for coal conversion and further explored below. Last but not least, it should be noted that the relative concentration of SO_2 formed via the side reactions of $CaSO_4$ as listed above was lower after adding CoO than those formed from YN reaction with the reference CoO and $CaSO_4$ or YN direct combustion in air, which was ascribed to effective fixation of the formed SO_2 as the solid sulfur compounds by the CoO included in the mixed OC. And the reaction mechanism involved would be further analyzed below.

Furthermore, based on the TG-DTG experimental data shown in Fig. 1 and previous studies on the direct combustion of coal in air [40,41], the flammability index C_r shown in Eq. (7) below was selected to quantitatively evaluate the chemical looping

combustion of YN lignite with the reference $CaSO_4$, CoO and its mixed OC.

$$C_r = \frac{(dw/dt)_{max}}{T_i^2} \quad (7)$$

Where $(dW/dt)_{max}$ was the maximal combustion rate of YN reaction with the mixed OC and its two reference oxides as described above, T_i was referred to the ignition temperature of the different reactions and determined using the TG-DTG method applied by many researchers [40,41], as shown in Fig. 1(b) with YN combustion in air as an example. According to Eq. (7), the higher flammability index C_r at the lower ignition temperature T_i meant a higher oxidation capacity of the oxidizing media adopted for coal conversion.

And then, according to Eq. (7), the flammability indexes of the YN reaction with air, the reference oxides $CaSO_4$, CoO and their mixed OC were calculated and presented in Fig. 3 below. The C_r value for YN reaction with air was the biggest and reached 3.09×10^{-5}, while its ignition temperature T_i was 323.56 °C and the lowest. After all, in relative to the $CaSO_4$–CoO mixed OC and its two reference oxides, air owned the highest oxidizing capacity for coal combustion, but a large fraction of N_2 was contained, which diluted the produced CO_2 stream with low concentration and was not easy to capture. Different from air, the C_r values of YN reaction with the CoO and $CaSO_4$ were as low as 4.84×10^{-6} and 7.87×10^{-6}, respectively. The lower C_r value of YN with CoO than that with $CaSO_4$ was mainly due to the inferior resistance to sintering for the unsupported single CoO, especially for its reduced elemental Co, though the reactivity of CoO reaction with YN was theoretically higher than that of $CaSO_4$, as analyzed in Fig. 1(c) above. And the characteristic ignition temperature T_i for YN reaction with CoO was determined as 367.26 °C, much lower than that of $CaSO_4$ with YN as 655.56 °C. Finally, for the as prepared $CaSO_4$–CoO mixed OC reaction with YN, as shown in Fig. 3 below, its C_r value was calculated as 1.74×10^{-5}, though only half of the C_r for YN combustion in air, but was greatly higher than those two C_r values for YN reaction with the two reference oxides, which fully indicated that modification of $CaSO_4$ by CoO using the combined preparation method owned higher reactivity for coal conversion. In the meantime, the ignition temperature T_i of the prepared mixed OC was 359.25 °C, still lower than that of YN with its two single reference oxides $CaSO_4$ and CoO, which was much advantageous for coal conversion in the real CLC process. Therefore, the prepared $CaSO_4$–CoO mixed OC was quite applicable to the real CLC process for efficient conversion of YN coal as well as CO_2 in-situ capture.

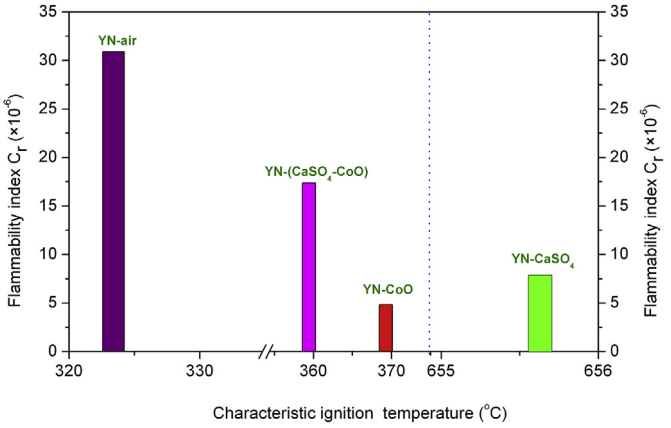

Fig. 3. The flammability indexes of the $CaSO_4$–CoO with YN coal.

3.2. FESEM-EDX and XRD analysis of the solid products of YN with the $CaSO_4$–CoO OC

After the research on the reaction of YN with the $CaSO_4$–CoO mixed OC by TGA-FTIR, in order to further clarify the reaction mechanisms, migration and redistribution of the sulfur species evolved from $CaSO_4$ during its reaction with YN, the morphologies of the solid residues of YN lignite reacting with the mixed $CaSO_4$–CoO and its two reference oxides, were characterized using FESEM, as shown in Fig. 4(a)-(d). Meanwhile, the elemental compositions at the optionally selected spots on the FESEM figures were listed in Table 2. In addition, crystalline phases involved were identified through XRD analysis, and presented in Fig. 5.

Firstly, for the morphology of the solid product of YN reaction with the reference $CaSO_4$, from Fig. 4(a), YN coal was observed not to sufficiently contact with $CaSO_4$ except at its external interfaces. In comparison with the shape of the $CaSO_4$ ore as studied [22], the reduced $CaSO_4$ shown in Fig. 4(a) is still plate-like and impervious with some channels etched on its surface. From the EDX analysis presented in Table 2, the atomic fraction of C left in spot 1 was 39.34%, a little higher than that in spot 2 with 26.33%, which illustrated that full conversion of YN lignite is difficult due to the lower reactivity of $CaSO_4$ ore and the insufficient contact between YN lignite and $CaSO_4$. From the XRD analysis of the reaction residues shown in Fig. 5(b), it also confirmed that in addition to the main reduced phase CaS, there were some unreacted $CaSO_4$ left. Meanwhile, the Ca atomic fractions on the two selected points was 24.63 and 15.40%, while the fractions of S left remained at 18.25 and 12.61%, respectively, which were lower than the concentration of Ca at the relevant points. And such a disparity between the Ca and S fractions was ascribed to the adverse effect of the gaseous sulfur emission via the side reactions mentioned above. As accompanied, a little CaO was formed as identified by the XRD analysis.

While for YN reaction with the reference CoO, as shown in Fig. 4(b), owing to the relatively inferior sintering resistance of the reduced Co, there existed discernible agglomerations of the Co grains on the outer surface of the unreacted CoO particles. Corresponding to the FESEM results, it could be observed that by the EDX analysis in Table 2, the C atomic concentrations on the point 1 and point 2 were 25.35 and 35.9%, respectively, much lower than that of YN reaction with $CaSO_4$. For the crystalline phases, the previous experiment and simulation had confirmed that the elemental Co was the main reduced product of the Co-based oxides in the reducing gases [42,43]. But the XRD analysis of the solid residue left after YN lignite reaction with CoO shown in Fig. 5(c) indicated that part of the CoO was not well reduced, which was mainly because the reduced Co grains of inferior sintering agglomerated on the outward surface as observed, causing the reducible gases evolved from YN coal were not easy to penetrate and well access the unreacted CoO inside. In addition, there was small part of undesired $CoAl_2O_4$ in the solid residues, which might arise from the interaction between the unreacted CoO and the aluminum-based mineral involved in YN coal at the high temperature [44].

Furthermore, after the reaction of YN with the mixed $CaSO_4$–CoO, the morphological feature as exhibited in Fig. 4(c) changed greatly. For the fresh $CaSO_4$–CoO particles prepared using the combined template method, the special core-shell structure was formed, similar to that of the $CaSO_4$–CuO in our previous research [22], where the doped CoO was densely distributed on the surface of the $CaSO_4$ substrate due to its steric confinement effect [45]. After reacting with YN lignite, the sharp edges of the $CaSO_4$ substrate in the mixed OC disappeared, and the CoO grains were more evenly distributed. According to the TG experiment results shown in Fig. 1 above, due to the higher reactivity of CoO than that of $CaSO_4$, it firstly reacted with YN coal to form Co, while the $CaSO_4$

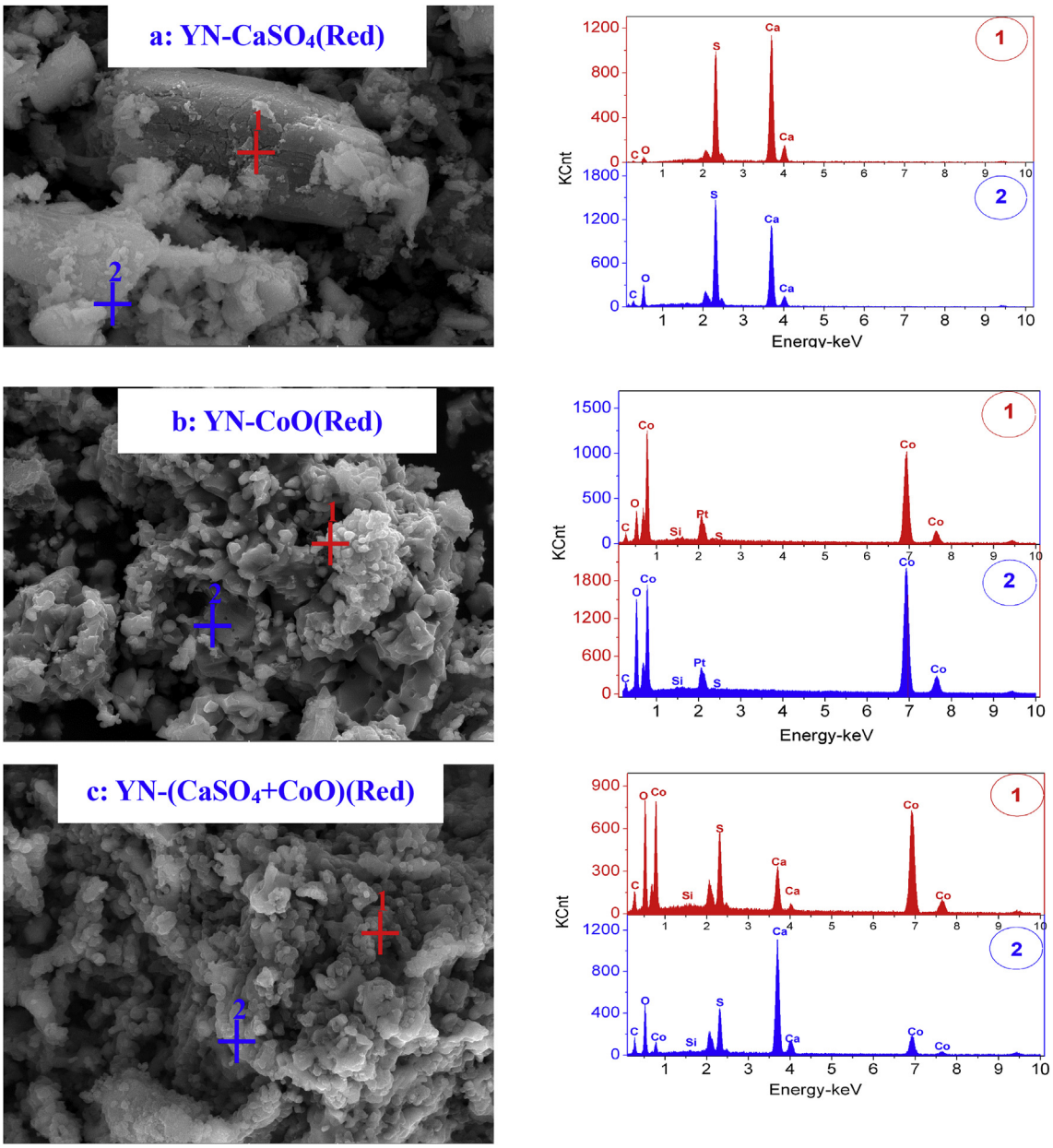

Fig. 4. FESEM-EDX analysis of the solid products: (a) YN reaction with $CaSO_4$; (b) YN reaction with CoO; (c) YN reaction with the $CaSO_4$–CoO mixed OC.

Table 2
Elemental analysis of the reaction of YN with $CaSO_4$–CoO by EDX (at%).

Sample		C	O	Si	Al	Co	Fe	S	Ca
YN-$CaSO_4$ (red)	Spot 1	39.34	17.11	0.08	0.18	0.00	0.41	18.25	24.63
	Spot 2	26.33	44.98	0.34	0.00	0.06	0.28	12.61	15.40
YN-CoO (red)	Spot 1	25.35	38.25	0.27	0.15	35.65	0.12	0.06	0.15
	Spot 2	35.90	21.49	0.91	0.37	40.70	0.42	0.09	0.12
YN-($CaSO_4$–CoO) (red)	Spot 1	14.36	39.93	0.16	0.11	9.37	0.08	14.06	21.93
	Spot 2	22.55	43.31	0.36	0.24	5.94	0.29	9.94	17.37

acted as the temporary inert support, preventing the agglomeration of the reduced Co grains and also providing sufficient surface area for reaction to continue, far different from YN reaction with the reference CoO as observed above. After the lattice oxygen in the CoO was consumed for coal conversion, $CaSO_4$ continued to transfer its oxygen involved for further conversion of the YN coal. Especially, due to the potential synergistic effect between these two components in the mixed OC, the reactivity of the mixed OC with YN coal was well enhanced. And thus, from Table 2, after YN reaction with the mixed $CaSO_4$–CoO, the atomic fractions of the residual C left were much lower than those from YN reaction with either CoO or $CaSO_4$, which further verified the higher reactivity of this mixed OC

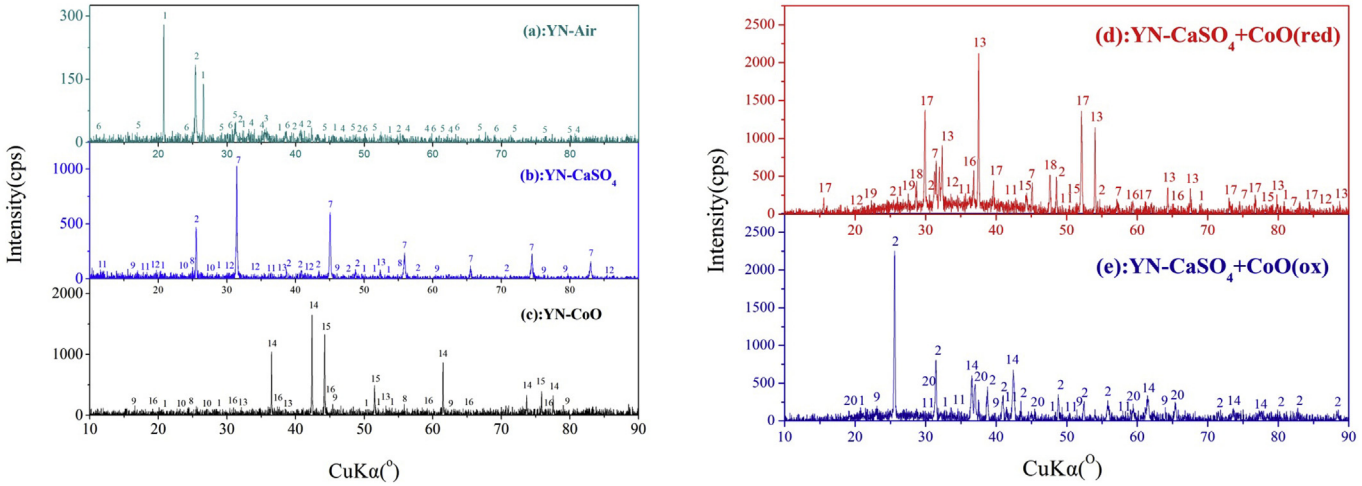

Fig. 5. XRD analysis of the solid products: (a) YN combustion in Air; (b) YN reaction with $CaSO_4$; (c) YN reaction with CoO; (d) YN reaction with the mixed $CaSO_4$–CoO; (e) Oxidation of the reduced $CaSO_4$–CoO.

to react with YN coal.

Finally, after the $CaSO_4$–CoO mixed OC reacted with YN lignite, the crystalline phases formed in the solid products were analyzed by XRD and shown in Fig. 5 below. From Fig. 5(a) for coal combustion by air, the crystalline phases involved were mainly identified as quartz (SiO_2), calcium sulfate ($CaSO_4$), hematite (Fe_2O_3) and various silicates. While for YN reaction with the reference $CaSO_4$, from Fig. 5(b), the reference $CaSO_4$ was mainly reduced to CaS with a little unreacted $CaSO_4$ left, mainly due to the low reactivity of $CaSO_4$ as well as insufficient contact of the plate-like $CaSO_4$ with YN coal, as analyzed above. And for YN reaction with the reference CoO, due to the inferior resistance to sintering of the firstly reduced Co on the unreacted CoO surface, which blocked the reducible gases from YN coal easily reach to the unreacted CoO inside. And thus, besides the reduced Co, some unreacted CoO was observed.

Far different from YN reaction with the two reference $CaSO_4$ and CoO above, as shown in Fig. 5(d), during YN reaction with the prepared $CaSO_4$–CoO mixed OC, the CoO contained in the mixed OC was firstly reduced to Co via Eq. (8) by various volatiles (such as H_2,CO,CH_4) emitted from YN pyrolysis [46]. According to the previous research [47], the reduced metal Co was capable of being further oxidized to Co_3O_4 by acceptance of the lattice oxygen transferred from the substrate $CaSO_4$ as shown in Eq. (9), especially across the eutectic interface between the unreacted $CaSO_4$ and the reduced CaS around 800–1000 °C [48]. And such a special oxygen recovery and transfer phenomena was also found in our previous researches on the reaction of YN with $CaSO_4$–CuO [22] and $CaSO_4$–Mn_3O_4 [28], which was quite advantageous for sufficient utilization of the oxygen inherent in the $CaSO_4$ for more efficient conversion of coal, and was well worthwhile a deeper exploration later.

$$CoO + H_2/CO/CH_4(g) \rightarrow Co + CO_2\,(g) + H_2O(g) \quad (8)$$

$$3Co + CaSO_4 \rightarrow Co_3O_4 + CaS \quad (9)$$

And then, the formed Co_3O_4 could directly decompose at high temperature, and the gaseous O_2 released would promote the direct combustion of the YN residual char left during the YN reaction with the $CaSO_4$–CoO mixed OC via reaction (10)–(11) below, similar to the combustion of the coal char by O_2 emitted from Co_3O_4 in the chemical looping oxygen uncoupling process [49]. Therefore, both the higher maximal reaction rate (shown in Fig. 1(d)) and the higher peak intensity of CO_2 (shown in Fig. 2(d)) were reached during the above TG-FTIR experiment. Meanwhile, as exhibited in Table 2, the EDX analysis of the solid products also indicated that the fractions of the remaining carbon left were lower after YN reaction with the prepared mixed OC.

$$2Co_3O_4 \rightarrow 6CoO + O_2(g) \quad (10)$$

$$C + O_2(g) \rightarrow CO_2(g) \quad (11)$$

As to the cobalt sulfides, including Co_9S_8 and CoS, as shown in Fig. 5(d), the possible reaction paths were explored as followed: the SO_2 formed from the side reactions of $CaSO_4$ in (1)–(5) was firstly reacted with the residual H_2 (referenced to Fig. 7(b) below) to form H_2S via the gaseous secondary reaction below [50].

$$SO_2(g) + 3H_2(g) \rightarrow H_2S(g) + 2H_2O(g) \quad (12)$$

And then, the generated H_2S in the reaction (12) would be favorably fixed by the reduced metal Co to form various solid cobalt sulfides (Co_9S_8 and CoS) [23].

In this figure, 1.quartz (SiO_2); 2.calcium sulfate ($CaSO_4$); 3.hematite (Fe_2O_3); 4.potassium aluminum silicate ($K_4Al_2SiO_9$); 5.calcium magnesium silicate (Ca_2MgSiO_7); 6.potassium aluminum sulfate ($KAl(SO_4)_2$); 7. oldhamite (CaS); 8.iron sulfide (FeS); 9.gehlenite ($Ca_2Al_2SiO_7$); 10.anorthite ($CaAl_2SiO_8$); 11.wollastonite ($CaSiO_3$); 12.tricalcium silicate (Ca_3SiO_5); 13.lime (CaO); 14.cobalt oxide (CoO); 15. cobalt(Co); 16. cobalt aluminum oxide ($CoAl_2O_4$); 17. cobalt sulfide (Co_9S_8); 18. cobalt sulfide(CoS); 19.calcium silicate (Ca_2SiO_4); 20. cobalt oxide(Co_3O_4).

In addition, full regeneration of the reduced OC was entailed as an essential demand of OC for its cyclic use in CLC. Therefore, the reduced $CaSO_4$–CoO mixed OC was further regenerated by exposure to the air, and the regenerated product was analyzed by XRD as shown in Fig. 5(e). The reduced OC was observed nearly completely regenerated to its original state with the main phases existing as $CaSO_4$ and CoO. In addition, a little SiO_2, $Ca_2Al_2SiO_7$ and $CaSiO_3$ could be also detected in the regenerated solid product due to the complex interaction of the reduced OC with the inherent minerals in YN. Negative consequence for deterioration of the OC reactivity and detrimental operation of the CLC system would be incurred.

And thus, separation of the coal ash out of the reduced OC was necessary in CLC, which would be focused and further studied in the future.

3.3. XPS identification of the solid species formed from YN reaction with the $CaSO_4$–CoO mixed OC

In order to more deeply ascertain the special oxygen transfer and recovery mechanism occurring at the metastable interface of the $CaSO_4$ during its reaction with YN coal, besides SEM-EDX and XRD analysis as conducted above, XPS was further adopted as a sensitive surface analysis means to obtain a more accurate insight into the composition and surface electronic state of the reduced $CaSO_4$–CoO mixed OC after its reaction with YN coal. The C 1s, O1s, Ca 2p and Co 2p XPS profiles as obtained were deconvoluted. And the related species were further determined according to the corresponding binding energy (BE), as shown in Fig. 6.

Full conversion of coal, especially the char left, is one of the vital goals to effectively capture CO_2 in the coal-fuelled CLC system [51,52]. Therefore, in order to reveal the limitation of the full conversion of coal at the atomic scale during its reaction with the mixed $CaSO_4$–CoO OC, the C 1s spectra were firstly analyzed to determine the carbon functional groups involved in the residue. As shown in Fig. 6(a), according to the relevant BE information related to the different carbon functional groups [53,54], the C 1s profile could be deconvoluted into four main peaks by curve-resolution, including the BE peak at 284.6eV for aliphatic or aromatic carbon (C–H or C–C), the BE value at 286.1eV for carbon bound to oxygen by the single bond (C–O) such as ether, phenol or alcohol, the peak at 287.8eV for the carbon bound to oxygen by the double bond (C=O) such as carbonyl group and the peak at 289.3 eV for the carbon bound to oxygen by the three bond (O=C–O). In addition, carbonate at the BE peak 290.5 eV existed as well [55]. Based on the fitted curve areas of the main carbon-containing functional groups as determined above, it was obvious that aliphatic or aromatic carbon functional groups were the key limitation for efficient conversion of YN coal from the atomic perspective.

Efficient utilization of the oxygen involved in the OC was important for coal conversion in CLC. From the O 1s XPS envelope shown in Fig. 5(b), after YN reaction with the $CaSO_4$–CoO mixed OC, it could be observed that the great contribution mainly resulted from various organic oxygen sources such as C=O groups at the BE value 531.4 eV and C–O groups at 532.9 eV. Apart from the contribution from these organic oxygen functional groups, various inorganic oxides could be identified as well. Such Co oxides as CoO and $CoAl_2O_4$ were observed with the BE peaks around 529.6 eV [56] and 530.8 eV [57], respectively. For the Ca-based oxides, a little $CaSO_4$ was detected in addition to the CaO produced by the $CaSO_4$ side reactions, with their BE value around 531.5 [58] and 530.3 eV [59], respectively. Furthermore, various silicon-containing

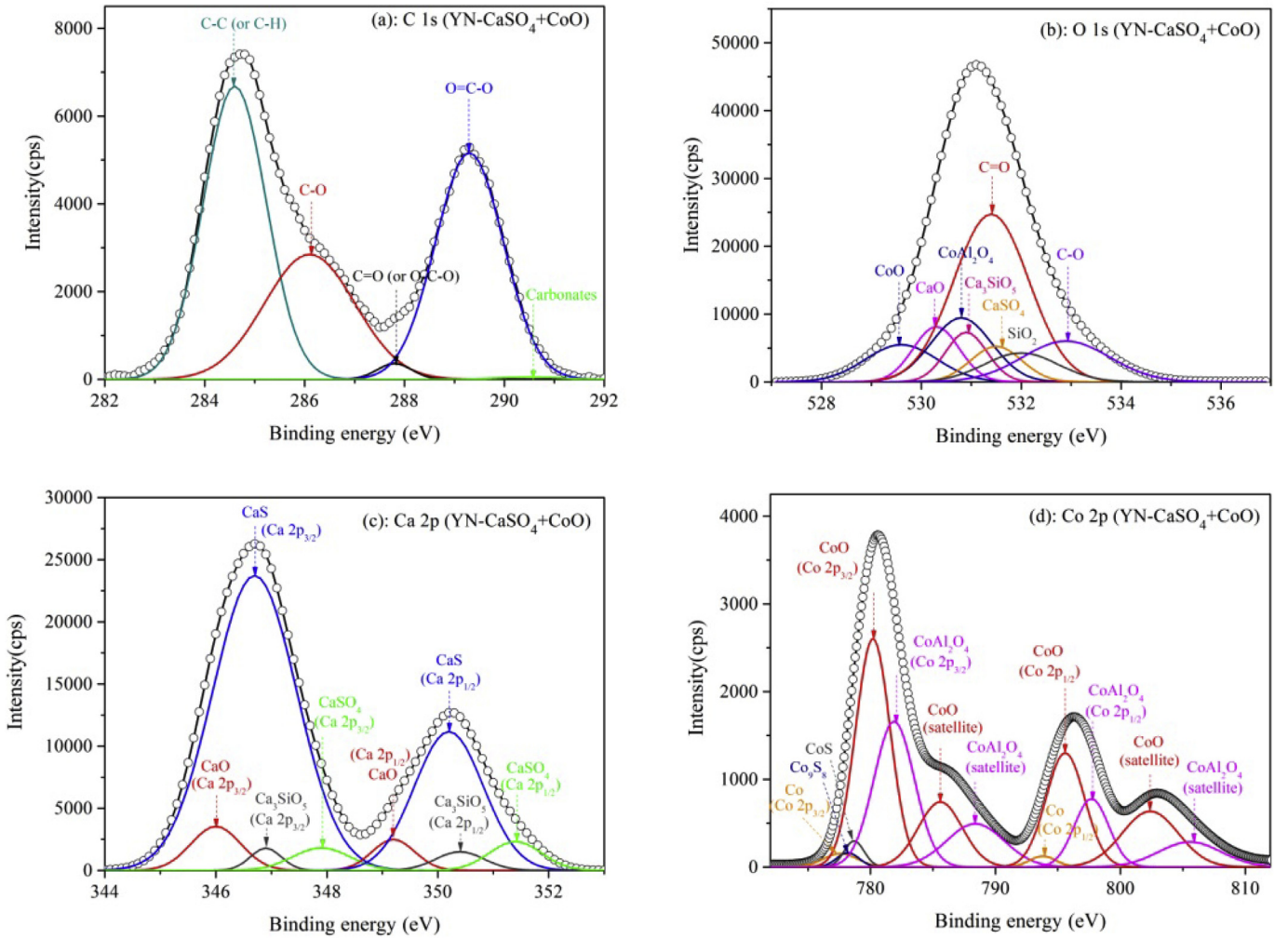

Fig. 6. XPS spectra of YN reaction with the $CaSO_4$–CoO mixed OC: (a) C 1s spectra; (b) O 1s spectra; (c) Ca 2p spectra; (d) Co 2p spectra.

compounds, including Ca_3SiO_5 at the BE value 530.9 eV [60] and SiO_2 at 532.0 eV [61], could be also observed in the O 1s profile, which agreed with the XRD analysis above.

For the Ca-based reduced products in the $CaSO_4$–CoO mixed OC, corresponding to the finding from the O 1s curve, CaO and $CaSO_4$ could be detected in the Ca 2p XPS profile of the solid residue [62] shown in Fig. 6(c). And the intensity of CaO was slightly higher than that of $CaSO_4$, implying that besides the main reduced counterpart CaS [63], some $CaSO_4$ was converted to CaO via the side reactions listed above. Meanwhile, the side product CaO would further react

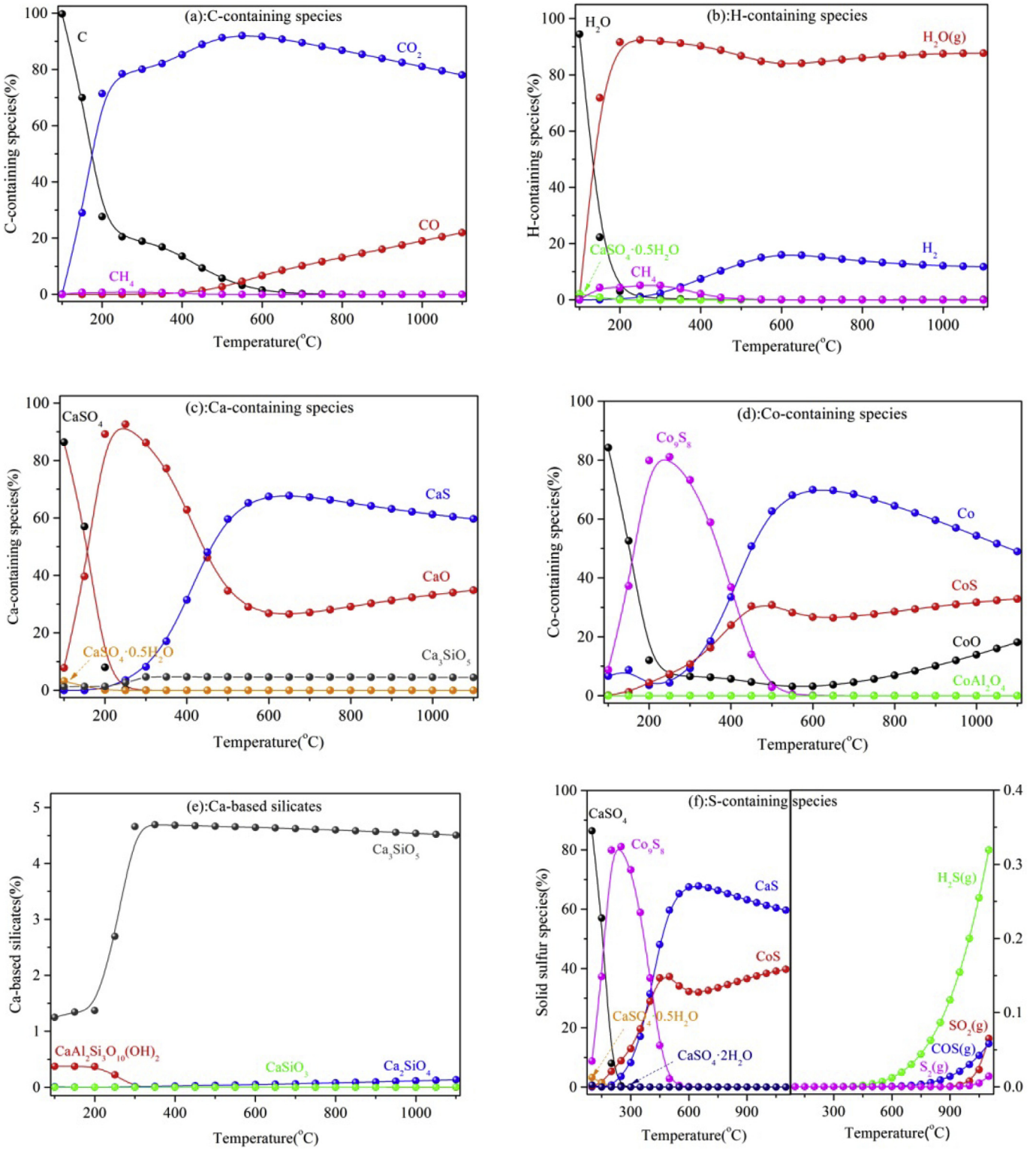

Fig. 7. Equilibrium distribution of various species for YN coal reaction with the $CaSO_4$–CoO mixed OC: (a) Carbon species; (b) Hydrogen species; (c) Calcium species; (d) Cobalt species; (e) Calcium-based silicates; (f) Various sulfur species.

with the active SiO_2 in YN to mainly form Ca_3SiO_5 with the BE value locating at 346.9 eV [60].

As to the reduced counterparts of the CoO in the $CaSO_4$–CoO mixed OC, as shown in Fig. 6(d) for the Co 2p XPS spectrum, two major Co-based compounds were determined as CoO and $CoAl_2O_4$ [56,63] and presented in Fig. 6(d). In addition, some cobalt sulfides, like Co_9S_8 and CoS, were also observed with their BE values around 778.2 [64] and 778.7 eV [65], respectively, which was consistent with the XRD analysis shown in Fig. 5(d). And elemental Co was found as well according to its BE values of Co $2p_{3/2}$ and Co $2p_{1/2}$ at 777.6 and 793.8 eV [66], respectively. Compared with CoO and $CoAl_2O_4$, Co content on the surface was quite low, which was different from XRD analysis above due to the sensitivity of elemental Co to oxidation [65] when exposed to the air.

3.4. Thermodynamic simulation of the $CaSO_4$–CoO mixed OC reaction with YN

Finally, in order to comprehensively learn the conversion of YN lignite, oxygen transfer of the mixed $CaSO_4$–CoO OC, transformation of the possible sulfur species and distribution of the main minerals, thermodynamic simulation of the $CaSO_4$–CoO reaction with YN lignite was conducted and presented in Fig. 7.

From Fig. 7(a), it could be observed that, with the oxidative disintegration of the main carbon structure of YN by the mixed $CaSO_4$–CoO, the carbon fraction declined sharply. And then above 300 °C, the residual carbon fraction was gradually decreased until stabilized below 1%. In correspondence, CO_2 was formed and dominant throughout the whole reaction. Nevertheless, a gradual decrease of CO_2 occurred with the reaction temperature increased from 600 °C upward. Due to the side reaction of $CaSO_4$ to form CaO as shown in Eqs. (1)–(6) above, some unburned CO was found over 500 °C with its fraction slowly increasing from 6.67% at 600 °C to 21.97% at 1100 °C. As to the evolution of H-containing species during YN coal reaction with the mixed OC, as shown in Fig. 7(b), besides the dominated H_2O, H_2 was also found to form when the reaction temperature was elevated to 300 °C. And then, the H_2 fraction was increased to 11.73% at 1100 °C.

As to the reduced counterparts of the prepared $CaSO_4$–CoO mixed OC during its reaction with YN, as shown in Fig. 7(c)–(d), the CoO and $CaSO_4$ included in the mixed OC were mainly reduced to Co and CaS. Meanwhile, a large amount of solid sulfides (such as Co_9S_8 and CoS) and CaO were found in the thermodynamic simulation, among which the Co_9S_8 and CoS mainly resulted from in-situ desulfurization of the gaseous sulfur emitted from the $CaSO_4$ side reactions. And further, as shown in Fig. 7(d), the former Co_9S_8 mainly formed below the relatively low temperature 500 °C, while the CoS mainly occurred above 500 °C, which was not in complete accordance with the XRD analysis in Fig. 5(d) above, mainly due to the limitation of the thermodynamic simulation as pointed above. While the CaO was derived from side reactions of $CaSO_4$ as shown in Eqs. (1)–(6) above, which could easily interact with the SiO_2 present in YN coal to form various silicates, as shown in Fig. 7(e). Among these silicates, Ca_3SiO_5 was dominated, in accordance with our solid product analysis above.

Furthermore, evolution and distribution of various sulfur species during the $CaSO_4$–CoO mixed OC reaction with YN was studied. From Fig. 7(f), at the reaction temperature of interest in CLC around 800–1000 °C, the main solid sulfur compounds were observed as CaS, CoS and Co_9S_8 with their total yield over 99.5%, which clearly indicated that the gaseous sulfur emitted from the $CaSO_4$ side reactions was effectively fixed as expected. Correspondingly, the possible harms of the gaseous SO_2 evolved from the side reactions of $CaSO_4$ [67] could be prevented. As to the formed solid sulfur compounds of CoS, Co_9S_8 and CaS, they could be easily separated and regenerated downstream through such measure as the post oxygen polishing. And then, the SO_2 formed was of high concentration and could be conveniently recovered for other industrial process, such as sulfuric acid production [68].

Finally, gaseous sulfur species (including SO_2 and H_2S as shown in Eqs. (1)–(6) above) emitted from $CaSO_4$ side reactions was always a great concern in CLC [11,12,17]. Therefore, under the precondition of efficient conversion of coal and cost-effective capture of the produced CO_2, in-situ desulfurization of the gaseous sulfur emitted from the $CaSO_4$ side reactions was much meaningful. Therefore, in order to simultaneously achieve in-situ decarbonation and desulfurization, effects of the reaction temperature, mass ratio of the $CaSO_4$ to CoO in the mixed OC and the OC oxygen excess number on the fixation of the gaseous sulfur were preliminarily studied. And the simulation results are shown in Fig. 8 below.

On the one hand, when the OC excess number was stabilized as the unity, the effect of the reaction temperature and the mass ratio of $CaSO_4$ to CoO on the fixation of the gaseous sulfur emission was studied and presented in Fig. 8(a). From Fig. 8(a), relative to the temperature 850 °C, the higher temperature benefited coal conversion during reaction with the $CaSO_4$ mixed OC of different

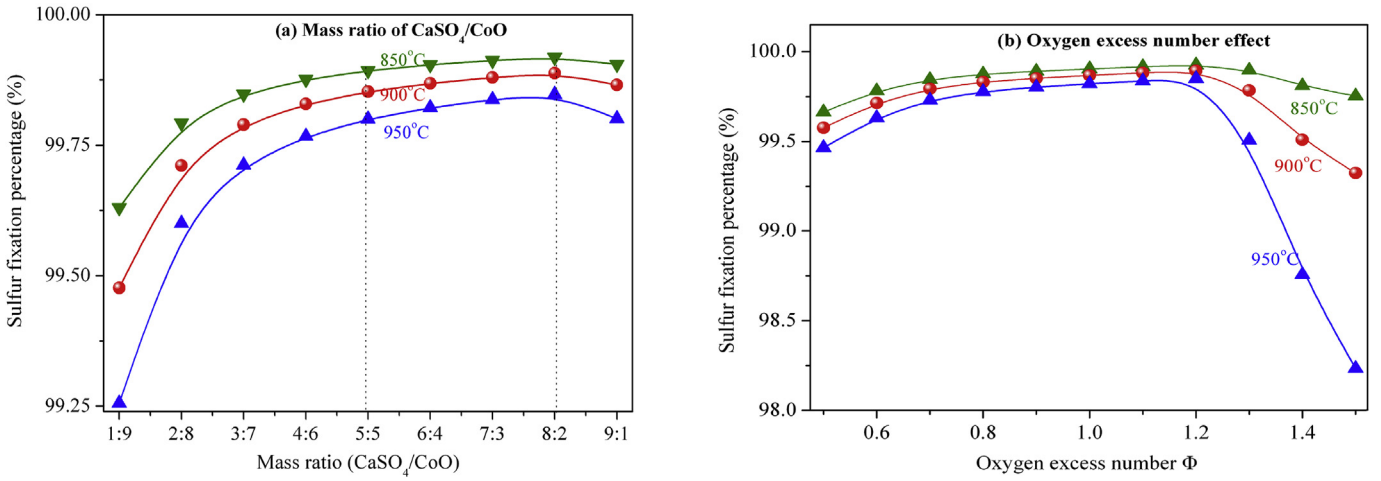

Fig. 8. Effect of the gaseous sulfur fixation by the different factors: (a) The reaction temperature, mass ratio of $CaSO_4$ to CoO in the mixed OC; (b) Effect of the oxygen excess number of the mixed OC.

$CaSO_4$/CoO mass ratios, but incurred more gaseous sulfur emission from the $CaSO_4$ side reaction [13,17,21], which was not favorable to fix the gaseous sulfur emitted. Meanwhile, the optimal content of CoO doped in the mixed $CaSO_4$–CoO OC was determined around 20–50% for efficient fixation of the emitted gaseous sulfur from the $CaSO_4$ side reactions. On the other hand, the OC excess number was one of the important parameters for CLC operation. And its effect on the gaseous sulfur emission from the $CaSO_4$ side reactions was further studied. As shown in Fig. 8(b), in order to fully convert YN coal and fix the emitted gaseous sulfur, for the fixed mass ratio of $CaSO_4$ to CoO as 6:4, the optimum mixed OC excess number was determined as 1.2.

In summary, according to the above thermodynamic simulation results, reaction temperature, oxygen excess number and mass ratio of the $CaSO_4$ to CoO in the mixed OC were the key factors affecting simultaneous in-situ decarbonation and desulfurization, which was of great significance to further study in the more realistic CLC process.

4. Conclusions

$CaSO_4$–CoO mixed OC was prepared using the combined method by integration of the template method with the sol-gel combustion synthesis (SGCS) procedure. The reaction characteristics of the prepared mixed OC with the typical lignite were evaluated by different experimental means in combination with the thermodynamic simulation. And the relevant conclusions are reached as followed:

(1) TGA analysis of YN reaction with the $CaSO_4$–CoO mixed OC displayed the desired reactivity of this mixed OC relative to its two reference components due to the beneficial synergistic effect of $CaSO_4$ decorated by CoO.
(2) SEM analysis of the morphological variation for the solid products of YN reaction with the mixed $CaSO_4$–CoO indicated the good resistance to sintering for this mixed OC due to the temporary support provided by the $CaSO_4$.
(3) XRD and XPS analysis of the solid residues from YN reaction with the mixed $CaSO_4$–CoO revealed that the lattice oxygen involved in the $CaSO_4$ could be transferred to the reduced Co via the particular interfacial reaction, thus effective utilization of the oxygen involved in the mixed OC could be realized for efficient conversion of coal.
(4) Finally, both gaseous FTIR analysis and the solid products characterization indicated that the gaseous sulfur species emitted from the side reaction of $CaSO_4$ were effectively fixed as the solid sulfur compounds, and thus in-situ decarbonization and desulfurization was simultaneously realized.

Acknowledgements

This work is supported by the National Natural Science Foundation of China (Nos. 51776073, 51276210), Key R&D program of Henan Province (Nos.162102210233), North China University of Water Resources and Electric Power (No.70481).

References

[1] J. Adanez, A. Abad, F. Garcia-Labiano, P. Gayan, F. Luis, Progress in chemical-looping combustion and reforming technologies, Prog. Energy Combust. Sci. 38 (2012) 215–282.
[2] S. Zhe, Z. Huang, High-efficiency and pollution-controlling in-situ gasification chemical looping combustion system by using CO_2 instead of steam as gasification agent, Chin. J. Chem. Eng. 26 (2018) 157–165.
[3] B.W. Wang, Y. Rong, Y. Zheng, H.B. Zhao, C.G. Zheng, Simulated investigation of chemical looping combustion with coal-derived syngas and $CaSO_4$ oxygen carrier, J. Fuel Chem. Technol. 39 (2011) 251–257.
[4] H. Zhao, L. Liu, B.W. Wang, D. Xu, L.L. Jiang, C.G. Zheng, Sol-gel-derived NiO/$NiAl_2O_4$ oxygen carriers for chemical-looping combustion by coal char, Energy Fuels 22 (2008) 898–905.
[5] L.H. Shen, J.H. Wu, Z.P. Gao, J. Xiao, Reactivity deterioration of NiO/Al_2O_3 oxygen carrier for chemical looping combustion of coal in a 10kW_{th} reactor, Combust. Flame 156 (2009) 1377–1385.
[6] N. Dilmaç, Ö.F. Dilmaç, E. Yardımci, Utilization of Menteş iron ore as oxygen carrier in chemical-looping combustion, Energy 138 (2017) 785–798.
[7] S. Zhang, S. Rajendran, R. Xiao, S. Bhattacharya, Chemical-looping combustion of Victorian brown coal using mixed oxygen carriers of iron and manganese oxides, Chemeca Challenging Tomorrow 7 (2013) 1–16.
[8] M. Tang, L. Xu, M. Fan, Progress in oxygen carrier development of methane-based chemical-looping reforming: a review, Appl. Energy 151 (2015) 143–156.
[9] E.H. Jeong, C.W. Nam, K.H. Park, J.H. Park, Sulfurization of Fe-Ni-Cu-Co alloy to matte phase by carbothermic reduction of calcium sulfate, Metall. Mater. Trans. B 47 (2016) 1103–1112.
[10] Q.J. Guo, J.S. Zhang, H.J. Tian, Recent advances in $CaSO_4$ oxygen carrier for chemical-looping combustion (CLC) process, Chem. Eng. Commun. 199 (2012) 1463–1491.
[11] S. Zhang, R. Xiao, J. Liu, S. Bhattachary, Performance of Fe_2O_3/$CaSO_4$ composite oxygen carrier on inhibition of sulfur release in calcium-based chemical looping combustion, Int. J. Greenhouse Gas Control 17 (2013) 1–12.
[12] T. Song, M. Zheng, L.H. Shen, T. Zhang, X. Niu, J. Xiao, Mechanism investigation of enhancing reaction performance with $CaSO_4$/Fe_2O_3 oxygen carrier in chemical-looping combustion of coal, Ind. Eng. Chem. Res. 52 (2013) 4059–4071.
[13] M. Zheng, L. Shen, X. Feng, In situ gasification chemical looping combustion of a coal using the binary oxygen carrier natural anhydrite ore and natural iron ore, Energy Convers. Manag. 83 (2014) 270–283.
[14] A. Abad, M. de Las Obras-Loscertales, F. García-Labiano, L. de Diego, P. Gayán, J. Adánez, In situ gasification Chemical-Looping Combustion of coal using limestone as oxygen carrier precursor and sulphur sorbent, Chem. Eng. J. 310 (2017) 226–239.
[15] S. Zhang, R. Xiao, Y. Yang, L. Chen, CO_2 capture and desulfurization in chemical looping combustion of coal with a $CaSO_4$ oxygen carrier, Chem. Eng. Technol. 36 (2013) 1469–1478.
[16] Q.J. Guo, X. Hu, Y.J. Liu, W.H. Jia, M. Yang, M. Wu, H. Tian, H.-J. Ryu, Coal chemical-looping gasification of Ca-based oxygen carriers decorated by CaO, Powder Technol. 275 (2015) 60–68.
[17] M. Zheng, Y. Xing, K. Li, S. Zhong, H. Wang, B. Zhao, Enhanced performance of chemical looping combustion of CO with $CaSO_4$-CaO oxygen carrier, Energy Fuels 31 (2017) 5255–5265.
[18] M. Zheng, L. Shen, J. Xiao, Reduction of $CaSO_4$ oxygen carrier with coal in chemical-looping combustion: effects of temperature and gasification intermediate, Int. J. Greenhouse Gas Control 4 (2010) 716–728.
[19] N. Ding, C. Zhang, C. Luo, Y. Zheng, Z. Liu, Effect of hematite addition to $CaSO_4$ oxygen carrier in chemical looping combustion of coal char, RSC Adv. 5 (2015) 56362–56376.
[20] N. Ding, Y. Zheng, C. Luo, C.G. Zheng, Effect of additives on $CaSO_4$ oxygen carrier in chemical-looping combustion, Proc. Chin. Soc. Electr. Eng. 31 (2011) 40–47.
[21] H.J. Tian, J. Chang, Q.J. Guo, Investigation into the reactivity behavior of $CaSO_4$ with coal chars in the chemical looping combustion System, Adv. Mater. Res. 724–725 (2013) 1158–1162.
[22] B. WWang, J. Li, N. Ding, D. Mei, H.B. Zhao, C.G. Zheng, Chemical looping combustion of a typical lignite with a $CaSO_4$–CuO mixed oxygen carrier, Energy Fuels 31 (2017) 13942–13954.
[23] J.B. Chung, J.S. Chung, Removal of sulfur fume by reactive absorption using cobalt-containing absorbents, Ind. Eng. Chem. Res. 43 (2004) 5318–5325.
[24] B.W. Wang, R. Yan, D.H. Lee, Y. Zheng, H.B. Zhao, C.G. Zheng, Characterization and evaluation of Fe_2O_3/Al_2O_3 oxygen carrier prepared by sol–gel combustion synthesis, J. Anal. Appl. Pyrolysis 91 (2011) 105–113.
[25] A. Huczko, Template-based synthesis of nanomaterials, Appl. Phys. A 70 (2000) 365–376.
[26] J.C. Hulteen, C.R. Martin, A general template-based method for the preparation of nanomaterials, J. Mater. Chem. 7 (1997) 1075–1087.
[27] B.W. Wang, H.B. Zhao, Y. Zheng, Z.H. Liu, C.G. Zheng, Chemical looping combustion of petroleum coke with $CuFe_2O_4$ as oxygen carrier, Chem. Eng. Technol. 36 (2013) 1488–1495.
[28] B.W. Wang, H.Y. Li, W. Wang, C. Luo, D.F. Mei, H.B. Zhao, Reaction characteristics investigation of the combined template method-made $CaSO_4$-Mn_3O_4 mixed oxygen carrier with lignite, Energy Fuels 33 (2019) 8954–8966.
[29] S.R. Jain, K.C. Adiga, A new approach to thermochemical calculations of condensed fuel-oxidizer mixtures, Combust. Flame 40 (1981) 71–79.
[30] B.W. Wang, Y.M. Cao, J. Li, W. Wang, H.B. Zhao, C.G. Zheng, Migration and redistribution of sulfur species during chemical looping combustion of coal with $CuFe_2O_4$ combined oxygen carrier, Energy Fuels 30 (2016) 8499–8510.
[31] B.W. Wang, R. Yan, H.B. Zhao, Y. Zheng, Z.H. Liu, C.G. Zheng, Investigation of chemical looping combustion of coal with $CuFe_2O_4$ oxygen carrier, Energy Fuels 25 (2011) 3344–3354.
[32] Y. Cao, B. Casenas, W.-P. Pan, Investigation of chemical looping combustion by solid fuels. 2. Redox reaction kinetics and product characterization with coal, biomass, and solid waste as solid fuels and CuO as an oxygen carrier, Energy Fuels 20 (2006) 1845–1854.

[33] L. Chen, J. Bao, L. Kong, M. Combs, H.S. Nikolic, Z. Fan, K. Liu, The direct solid-solid reaction between coal char and iron-based oxygen carrier and its contribution to solid-fueled chemical looping combustion, Appl. Energy 184 (2016) 9–18.
[34] R. Siriwardane, H. Tian, T. Simonyi, G. Richards, Chemical-looping combustion of coal with metal oxide oxygen carriers, Energy Fuels 23 (2009) 3885–3892.
[35] Y. Zheng, Mechanism study of wood lignin pyrolysis by using TG–FTIR analysis, J.Anal.Appl.pyrolysis 82 (2008) 170–177.
[36] B.W. Wang, M. Qiang, W. Wang, C. Zhang, D. Mei, H. Zhao, C.G. Zheng, Effect of reaction temperature on the chemical looping combustion of coal with $CuFe_2O_4$ combined oxygen carrier, Energy Fuels 31 (2017) 5233–5245.
[37] S. Sebbahi, M.L.O. Chameikh, F. Sahban, J. Aride, L. Benarafa, L. Belkbir, Thermal behaviour of Moroccan phosphogypsum, Thermochim. Acta 302 (1997) 69–75.
[38] S. Yang, D.K. Zhang, An experimental study of sulphate transformation during pyrolysis of an Australian lignite, Fuel Process. Technol. 91 (2010) 313–321.
[39] Z. Da, H. Lu, X. Sun, X. Liu, W. Han, L. Wang, Reaction mechanism of reductive decomposition of FGD gypsum with anthracite, Thermochim. Acta 559 (2013) 23–31.
[40] J. Chen, X. Sun, Determination of the devolatilization index and combustion characteristic index of pulverized coals, Power Eng. 5 (1987) 15–20+63.
[41] J. Zhou, H. Zhang, L. Junfu, Study on combustion characteristics of a petroleum coke at different heating rates by using thermogravimetry, Coal Convers 29 (2006) 39–43.
[42] H. Alalwan D. Cwiertny, V.H. Grassian, Co_3O_4 nanoparticles as oxygen carriers for chemical looping combustion:A materials characterization approach to understanding oxygen carrier performance, Chem. Eng. J. 319 (2017) 279–287.
[43] B.W. Wang, C.C. Gao, W. Wang, F. Kong, C. Zheng, TGA-FTIR investigation of chemical looping combustion by coal with $CoFe_2O_4$ combined oxygen carrier, J. Anal. Appl. Pyrolysis 105 (2014) 369–378.
[44] Y. Okamoto, T. Adachi, K. Nagata, M. Odawara, T. Imanaka, Effects of starting cobalt salt upon the cobalt-alumina interactions and hydrodesulfurization activity of CoO/Al_2O_3, Appl. Catal. 73 (1991) 249–265.
[45] Q. Fan, J. Dai, T. Wang, J. Kuttner, G. Hilt, J.M. Gottfried, J. Zhu, Confined synthesis of organometallic chains and macrocycles by Cu-O surface templating, ACS Nano 10 (2016) 3747–3754.
[46] L. Wang, W. Qin, X. Xiao, Z. Zheng, J. Zhang, C. Dong, Y. Yang, Effect of Co-doping on iron-based oxygen carrier for CO oxidation in chemical looping combustion, Adv. Mater. Res. 774–776 (2013) 725–728.
[47] C. Doornkamp, V. Ponec, The universal character of the Mars and Van Krevelen mechanism, J. Mol. Catal. A Chem. 162 (2000) 19–32.
[48] N.H. Davies, A. Hayhurst, On the formation of liquid melts of CaS and $CaSO_4$ and their importance in the absorption of SO_2 by CaO,Combust, Flame 106 (1996) 359–362.
[49] T. Mattisson, A. Lyngfelt, H. Leion, Chemical-looping with oxygen uncoupling for combustion of solid fuels, Int. J. Greenhouse Gas Control 3 (2009) 11–19.
[50] D.M. Fenton, H.W. Gowdy, The chemistry of the Beavon sulfur removal process, Environ. Int. 2 (1979) 183–186.
[51] L.H. Shen, J.H. Wu, J. Xiao, Experiments on chemical looping combustion of coal with a NiO based oxygen carrier, Combust. Flame 156 (2009) 721–728.
[52] N. Berguerand, A. Lyngfelt, Design and operation of a $10kW_{th}$ chemical-looping combustor for solid fuels-Testing with South African coal, Fuel 87 (2008) 2713–2726.
[53] R. Pietrzak, T. Grzybek, H. Wachowska, XPS study of pyrite-free coals subjected to different oxidizing agents, Fuel 86 (2007) 2616–2624.
[54] D.L. Perry, A. Grint, Application of XPS to coal characterization, Fuel 62 (1983) 1024–1033.
[55] R. Fiedler D. Bendler, ESCA investigations on Schleenhain lignite lithotypes and the hydrogenation residues, Fuel 71 (1992) 381–388.
[56] V. An Du, S. Gross, U. Schubert, Re-investigation of the thermal decomposition of $Co(CO)_4SiCl_3$ adsorbed on silica, Chem. Commun. 46 (2010) 8549–8551.
[57] T.A. Patterson, J.C. Carver, D.E. Leyden, D.M. Hercules, A surface study of cobalt-molybdena-alumina catalysts using X-ray photoelectron spectroscopy, J. Phys. Chem. 80 (1976) 1700–1708.
[58] B. Demri, D. Muster, XPS study of some calcium compounds, J. Mater. Process. Technol. 55 (1995) 311–314.
[59] H. Lu, P. Smirniotis, Calcium oxide doped sorbents for CO_2 uptake in the presence of SO_2 at high temperatures, Ind. Eng. Chem. Res. 48 (2009) 5454–5459.
[60] M. Regourd, J.-H. Thomassin, P. Baillif, J.C. Touray, Study of the early hydration of Ca_3SiO_5 by X-ray photoelectron spectrometry, Cement Concr. Res. 10 (1980) 223–230.
[61] R.V. Siriwardane, J.M. Cook, Interactions of NO and SO_2 with iron deposited on silica, J. Colloid Interface Sci. 104 (1985) 250–257.
[62] M.I. Sosulnikov, Y. Teterin, X-ray photoelectron studies of Ca, Sr and Ba and their oxides and carbonates, J. Electron. Spectrosc. Relat. Phenom. 59 (1992) 111–126.
[63] H. Franzen, J. Merrick, M. Umaña, A.S. Khan, D.T. Peterson, J.R. McCreary, R.J. Thorn, XPS spectra and crystalline in Alkaline-Earth chalcogenides and hybrides, J. Electron. Spectrosc. Relat. Phenom. 11 (1977) 439–443.
[64] Q. Liu, J. Zhang, A general and controllable synthesis of ComSn (Co_9S_8, Co_3S_4, and $Co_{1-x}S$) hierarchical microspheres with homogeneous phases, CrystEngComm 15 (2013) 5087–5092.
[65] J. Liu, Y. Xing, X. Liu, X. Yu, Z. Su, Hydrothermal synthesis and magnetic properties of nanoplate-assembled hierarchical structured $Co_{1-x}S$ microrods, Mater. Char. 67 (2012) 112–118.
[66] S. Velu, K. Suzuki, Photoemission and in situ XRD investigations on CuCoZnAl-mixed metal oxide catalysts for the oxidative steam reforming of methanol, J. Phys. Chem. B 106 (2002) 12737–12746.
[67] A. Aspelund, K. Jordal, Gas conditioning-The interface between CO_2 capture and transport, Int. J. Greenhouse Gas Control 1 (2007) 343–354.
[68] F. García-Labiano, L.F.D. Diego, A. Cabello, P. Gayán, A. Abad, J. Adánez, G. Sprachmann, Sulphuric acid production via chemical looping combustion of elemental sulphur, Appl. Energy 178 (2016) 736–745.